Article

The cool brown dwarf Gliese 229 B is a close binary

https://doi.org/10.1038/s41586-024-08064-x

Received: 2 July 2024

Accepted: 17 September 2024

Published online: 16 October 2024

Check for updates

Jerry W. Xuan[1✉], A. Mérand[2,34], W. Thompson[3,34], Y. Zhang[1], S. Lacour[2,4], D. Blakely[3,5], D. Mawet[1,6], R. Oppenheimer[7], J. Kammerer[2], K. Batygin[8], A. Sanghi[1], J. Wang[9,10], J.-B. Ruffio[11], M. C. Liu[12], H. Knutson[8], W. Brandner[13], A. Burgasser[11], E. Rickman[14], R. Bowens-Rubin[15], M. Salama[15], W. Balmer[16], S. Blunt[9,10], G. Bourdarot[17], P. Caselli[17], G. Chauvin[18], R. Davies[17], A. Drescher[17], A. Eckart[19,20], F. Eisenhauer[17], M. Fabricius[17], H. Feuchtgruber[17], G. Finger[17], N. M. Förster Schreiber[17], P. Garcia[21,22], R. Genzel[17], S. Gillessen[17], S. Grant[17], M. Hartl[17], F. Haußmann[17], T. Henning[13], S. Hinkley[23], S. F. Hönig[24], M. Horrobin[19], M. Houllé[18], M. Janson[25], P. Kervella[4], Q. Kral[4], L. Kreidberg[13], J.-B. Le Bouquin[26], D. Lutz[17], F. Mang[17], G.-D. Marleau[13,27,28,29], F. Millour[18], N. More[17], M. Nowak[30], T. Ott[17], G. Otten[31], T. Paumard[4], S. Rabien[17], C. Rau[17], D. C. Ribeiro[17], M. Sadun Bordoni[17], J. Sauter[13], J. Shangguan[17], T. T. Shimizu[17], C. Sykes[24], A. Soulain[26], S. Spezzano[17], C. Straubmeier[19], T. Stolker[32], E. Sturm[17], M. Subroweit[19], L. J. Tacconi[17], E. F. van Dishoeck[17], A. Vigan[33], F. Widmann[17], E. Wieprecht[17], T. O. Winterhalder[2] & J. Woillez[2]

Owing to their similarities with giant exoplanets, brown dwarf companions of stars provide insights into the fundamental processes of planet formation and evolution. From their orbits, several brown dwarf companions are found to be more massive than theoretical predictions given their luminosities and the ages of their host stars[1–3]. Either the theory is incomplete or these objects are not single entities. For example, they could be two brown dwarfs each with a lower mass and intrinsic luminosity[1,4]. The most problematic example is Gliese 229 B (refs. 5,6), which is at least 2–6 times less luminous than model predictions given its dynamical mass of 71.4 ± 0.6 Jupiter masses (M_{Jup}) (ref. 1). We observed Gliese 229 B with the GRAVITY interferometer and, separately, the CRIRES+ spectrograph at the Very Large Telescope. Both sets of observations independently resolve Gliese 229 B into two components, Gliese 229 Ba and Bb, settling the conflict between theory and observations. The two objects have a flux ratio of 0.47 ± 0.03 at a wavelength of 2 μm and masses of 38.1 ± 1.0 and 34.4 ± 1.5 M_{Jup}, respectively. They orbit each other every 12.1 days with a semimajor axis of 0.042 astronomical units (AU). The discovery of Gliese 229 BaBb, each only a few times more massive than the most massive planets, and separated by 16 times the Earth–moon distance, raises new questions about the formation and prevalence of tight binary brown dwarfs around stars.

Gliese 229 B, the first brown dwarf with methane-absorption features[5,6], orbits the M1V star Gliese 229 A (0.58 ± 0.01 $M_{\odot}$) with a semimajor axis of 33 AU (ref. 1). The powerful combination of Gaia DR3 and Hipparcos astrometry, as well as decades of imaging and radial velocity (RV) monitoring of the host star, enable a precise dynamical mass measurement of 71.4 ± 0.6 M_{Jup} for the companion[1]. The high mass of Gliese 229 B has defied all existing substellar evolutionary models, which predict that a 71.4-M_{Jup} object with age from 1 to 10 Gyr would have a bolometric luminosity about 2–20 times higher than the measured value of $\log(L/L_{\odot}) = -5.21 \pm 0.05$ (refs. 1,7–9) (see Fig. 3 and Extended Data Fig. 1). In fact, for models that include clouds, 71.4 M_{Jup} is near the hydrogen-burning limit (at solar metallicity) that defines the substellar–stellar boundary[10] (ref. 8: 73.3 M_{Jup}; ref. 11: 70.2 M_{Jup}). The mass–luminosity discrepancy for Gliese 229 B raises questions about the accuracy of the models, which has serious implications, as these models are used to infer masses for most of the directly imaged giant planets and brown dwarf companions that lack dynamical masses.

Alternatively, the low luminosity of brown dwarf companions such as Gliese 229 B could be explained if they consist of a spatially unresolved pair of brown dwarfs instead of a single one[1–4]. Other indications of the unusual nature of Gliese 229 B include its near-infrared spectrum, which does not conform to spectral standards, prompting Burgasser et al.[12] to assign it a spectral type of peculiar T7. Despite these anomalies, past observations have unsuccessfully attempted to resolve Gliese 229 B into a binary brown dwarf with adaptive optics imaging[13]. The previous non-detections along with the proximity of the system (5.76 parsec from Gaia[14]) suggest that a putative binary would have a tight separation of <0.2 AU or a small mass ratio[1]. However, known binary brown dwarfs show a strong preference for equal mass ratios and a separation distribution peaking between approximately 1 and 3 AU (refs. 15,16).

A list of affiliations appears at the end of the paper.

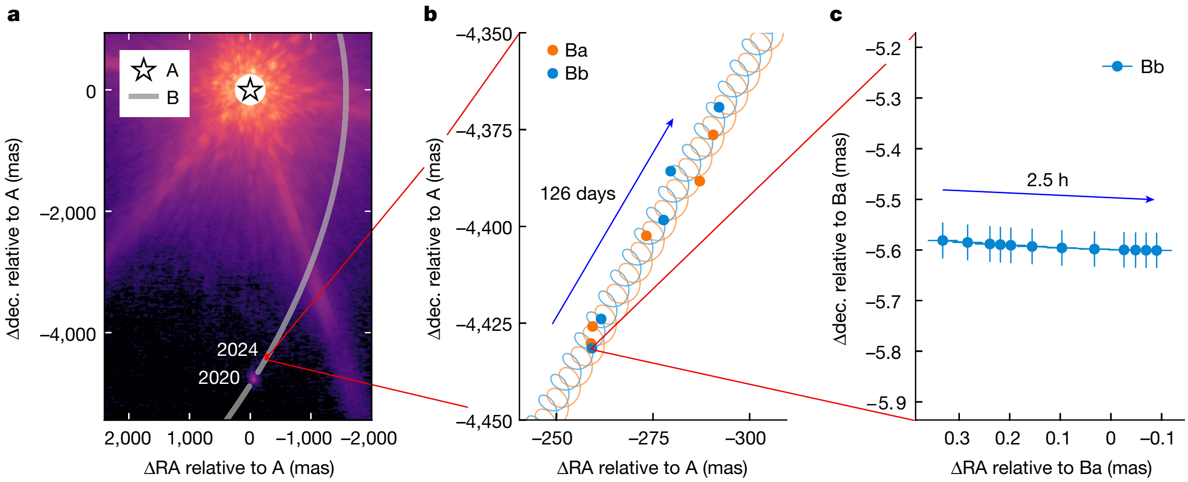

Fig. 1 | The detection and astrometric orbit of Gliese 229 BaBb. **a**, A Keck/NIRC2 K_s band image of the Gliese 229 system taken on 18 October 2021. The binary brown dwarf is unresolved given Keck's resolution of 45 mas. The grey line indicates the best estimate of the outer orbit of Gliese 229 BaBb around A (ref. 1). **b**, A zoom-in for the maximum a posteriori binary brown dwarf orbit from the GRAVITY and CRIRES+ joint fit, in which the measured positions of Gliese 229 Ba and Bb in each GRAVITY epoch are shown as orange and blue points, respectively. The average uncertainty on the derived relative position between Bb and Ba is between 0.01 and 0.05 mas. Note that GRAVITY and CRIRES+ only measure the differential positions between Ba and Bb, so the length and direction of the spiral pattern are derived from the maximum a posteriori draw of the outer orbit (grey line in panel **a**). **c**, The motion of Gliese 229 Bb relative to Gliese 229 Ba during the 2.5-h observing window of the first night of GRAVITY observations.

We observed Gliese 229 B on five nights using the Very Large Telescope Interferometer (VLTI) in GRAVITY Wide mode[17] with the Unit Telescopes of the European Southern Observatory (ESO) at Cerro Paranal, Chile. The observations were performed in the K band (1.95–2.45 μm). We extracted closure phases from the GRAVITY data (see Methods), in which a non-zero closure phase indicates a departure from central symmetry, for example, a binary source. As part of the same programme, we observed Gliese 229 B with the CRyogenic

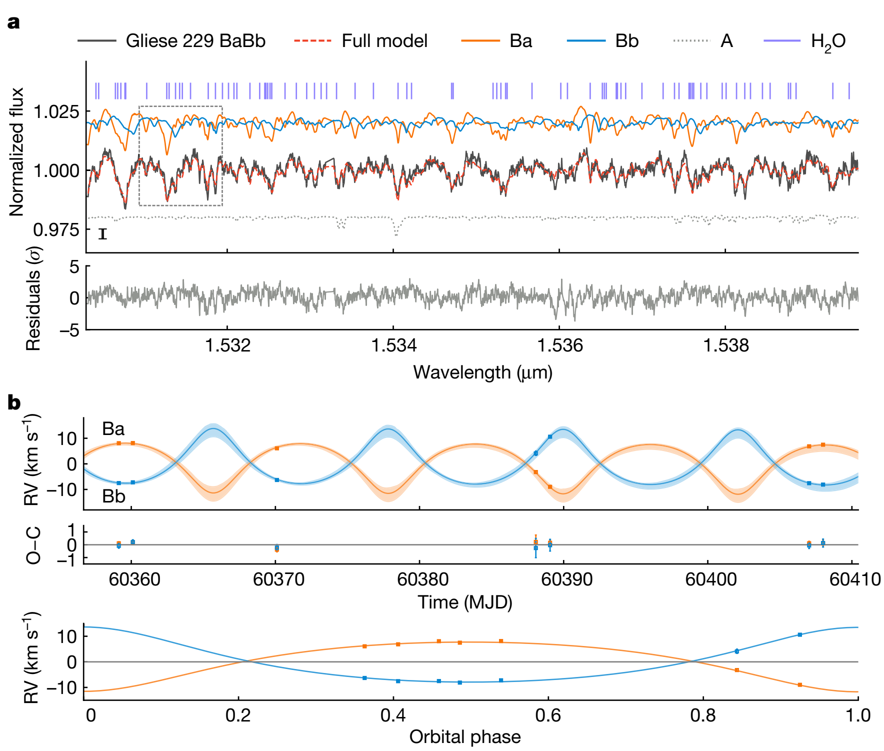

Fig. 2 | CRIRES+ spectrum and spectroscopic orbit of Gliese 229 Ba and Bb. **a**, A segment of the CRIRES+ spectrum from 20 March 2024 (black) used to compute RVs of Gliese 229 Ba and Bb. The region is dominated by water-absorption lines from the brown dwarfs, whose positions are marked in purple. The orange and blue curves are spectral models for Ba and Bb, respectively, and the dashed grey curve is the CRIRES+ spectra of Gliese 229 A used to model stellar contamination. The three model components have been offset for clarity. The full model is shown in red. The median uncertainty of the spectrum is denoted by the 1σ error bar at the lower left. In the grey box, we highlight a region in which distinct lines from Ba and Bb can be identified by eye. **b**, The orange and blue points show the RVs of Gliese 229 Ba and Bb, respectively, extracted from seven epochs of VLT/CRIRES+ spectra. Solid lines denote the joint CRIRES+ and GRAVITY orbit fit, with 2σ uncertainty regions shaded. The middle panel shows the residuals of the best fit and the bottom panel shows the phase-folded RV orbit.

InfraRed Echelle Spectrograph Upgrade Project (CRIRES+)[18] on UT3 of the Very Large Telescope in the H band (1.50–1.75 μm) on seven different nights to monitor its RV. The CRIRES+ spectra have a resolving power ($\lambda/\Delta\lambda$) of about 100,000 and were extracted as described in Methods.

We find strongly non-zero closure phases in the first epoch of GRAVITY observations (Extended Data Fig. 2) that are consistent with a binary source. The subsequent GRAVITY epochs confirm the detection and provide evidence of orbital motion between the two components (Fig. 1). With the first epoch alone, the null hypothesis that Gliese 229 B is a single source (that is, all closure phases should be zero) leads to a reduced χ^2 of 55 (288 degrees of freedom). Carrying out a grid search for the companion as described in ref. 19, we find a secondary brown dwarf located approximately 5 mas south of the brighter, primary brown dwarf, with a secondary-to-primary flux ratio of about 0.5. The binary fit has a much lower reduced χ^2 of 1.27. In the binary fit, we also account for linear motion of the companion over the 2.5-h observing window. We find that the companion moves in a direction nearly perpendicular to the vector between itself and the brighter brown dwarf at a rate of $4.6^{+1.5}_{-0.8}$ mas day^{-1} (Fig. 1c), consistent with the expected motion of approximately 4.6 mas from a circular, face-on orbit for a total mass of 71 $M_{\rm Jup}$.

Contemporaneous CRIRES+ monitoring independently confirms that Gliese 229 B is a binary brown dwarf. Initially, we cross-correlated the CRIRES+ spectra of Gliese 229 B with a Sonora Elf Owl atmospheric model[20] assuming $T_{\rm eff}$ = 900 K and log(g) = 5.0 (ref. 21). The cross-correlation functions (CCFs) showed time-varying line locations and shapes consistent with the partially resolved spectra of two brown dwarfs orbiting each other (Extended Data Figs. 3 and 4). Therefore, we fit the CRIRES+ spectra as emission from two brown dwarfs and account for a small amount of starlight leakage into the slit using observations of Gliese 229 A (Fig. 2a; see Methods). On the basis of the GRAVITY-measured flux ratio, we started with atmospheric models with $T_{\rm eff}$ = 850 K and log(g) = 5 for the primary brown dwarf and $T_{\rm eff}$ = 750 K and log(g) = 5 for the secondary brown dwarf (see Methods) to extract the RV of each brown dwarf. For each CRIRES+ epoch, alternative fits of the spectra with a single-component brown dwarf model are disfavoured with statistical significance ≥20σ. The extracted RVs show unambiguous signs of a spectroscopic binary (Fig. 2b).

We combine the CRIRES+ and GRAVITY data to characterize the orbit of the binary brown dwarf. The orbit fits are performed with PMOIRED[22] and Octofitter[23], as described in Methods. The data are well fit by the model with a reduced χ^2 of 2.2 (513 degrees of freedom) and slightly broad but symmetrical closure phase residuals, with the model accounting for all closure phase features. The GRAVITY K band flux ratio is constrained by the joint fit to 0.47 ± 0.03. We derive an orbital period of 12.134 ± 0.003 days, corresponding to a semimajor axis of 0.0424 ± 0.0004 AU, or about 90 Jupiter radii. The ratio of the RV semiamplitudes directly constrains the mass ratio (q) to $0.90^{+0.06}_{-0.02}$. From the orbit of the binary brown dwarf, we independently measure a total mass of 72.5 ± 1.3 $M_{\rm Jup}$, which is consistent with the mass derived in ref. 1 from the orbit of the unresolved Gliese 229 B around Gliese 229 A. We measure component masses of 38.1 ± 1.0 $M_{\rm Jup}$ and 34.4 ± 1.5 $M_{\rm Jup}$, an eccentricity of 0.234 ± 0.004 and inclination of 31.4 ± 0.3° (see Table 1). The eccentricity of Gliese 229 Bab is typical compared with the eccentricity distribution of field binary brown dwarfs[24]. We note that the outer orbit of Gliese 229 Bab around Gliese 229 A is highly eccentric ($e \approx 0.85$) and viewed nearly face-on[1]. The orbit of the binary brown dwarf is moderately misaligned relative to the outer orbit by 37^{+7}_{-10}°. Furthermore, the spin orientation of the host star is viewed nearly edge-on[25] and therefore misaligned relative to both inner and outer orbits.

To make the astrometric and spectroscopic observations fully self-consistent with the atmosphere models, we interpolate the

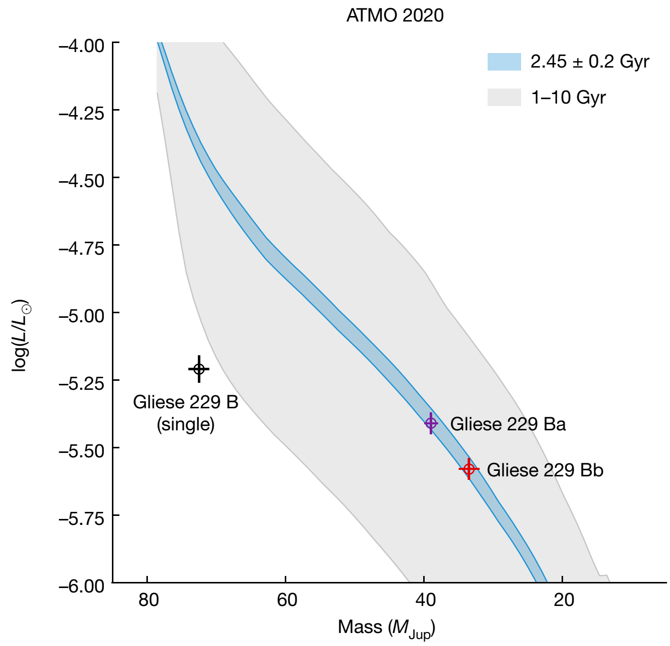

Fig. 3 | Dynamical masses and inferred luminosities of Gliese 229 Ba and Bb from ATMO 2020. The dynamical masses from our orbit fit and inferred luminosities of Gliese 229 Ba (purple) and Bb (red) from the ATMO 2020 evolutionary model. As a single brown dwarf, Gliese 229 B is under-luminous compared with model predictions for all plausible ages of the system from ref. 13. The mass–luminosity tension is also present for other models (see Extended Data Fig. 1). As a binary brown dwarf, the system is well explained by the ATMO 2020 model for an age of 2.45 ± 0.20 Gyr, resolving the mass–luminosity tension.

ATMO 2020 substellar evolutionary model[9,26] to search for component masses and ages that simultaneously reproduce the GRAVITY K band flux ratio and bolometric luminosity (see Methods). Adopting a prior on the total mass of 72.5 ± 1.3 $M_{\rm Jup}$, we find that a binary brown dwarf with mass ratio 0.87 ± 0.03 and age 2.45 ± 0.20 Gyr matches the models well. This mass ratio is consistent at the 1σ level with the value derived from the orbit fit. From ATMO 2020, the primary component is estimated to have $T_{\rm eff}$ = 860 ± 20 K, log(g) = 5.11 ± 0.01 dex and log($L/L_{\odot}$) = −5.41 ± 0.04, whereas the secondary component has $T_{\rm eff}$ = 770 ± 20 K, log(g) = 5.03 ± 0.01 dex and log($L/L_{\odot}$) = −5.58 ± 0.04. Our inferred age agrees with the value of about 2–6 Gyr estimated for the host star[13]. Therefore, our detection of the binary and measurements of its properties bring the system into much better alignment with substellar evolutionary models, as shown in Fig. 3.

Although the near-unity mass ratio between Gliese 229 Ba and Bb fits with previous binary brown dwarfs[16], the semimajor axis of approximately 0.042 AU makes it the tightest binary brown dwarf in a triple system (Extended Data Fig. 5). Among binary brown dwarfs orbiting stars, the next closest binaries have semimajor axis values more than an order of magnitude larger at about 0.9 AU (for example, Gliese 569 Bab (ref. 24)). Several isolated ultracool dwarf binaries with component masses between 0.08 and 0.09 $M_{\odot}$ have smaller separations[27,28], but among unambiguous binary brown dwarfs, only 2MASS J0535−0546AB and SPEC J1510−2818AB have comparable separations of 0.04 and 0.06 AU, respectively[29,30]. The formation mechanism of binary brown dwarfs around stars remains an open question, and both observations and simulations are highly incomplete for binary brown dwarfs with separations <1 AU (ref. 15). Opacity-limited fragmentation restricts the primordial separations of objects to distances >10 AU (ref. 31), implying that substantial dynamical and dissipative processes are required to form tight binary brown dwarf systems[32]. Although the

Table 1 | Orbital and physical parameters of Gliese 229 BaBb

	Confidence interval (frequentist analysis): median and 16th–84th percentiles	Credible interval (Bayesian analysis): median and 16th–84th percentiles
Orbital period (days)	12.134±0.003	12.137±0.001
Semimajor axis (AU)	0.0424±0.0004	0.0422±0.0001
Eccentricity	0.234±0.004	0.234±0.002
Argument of periastron (°)	180.7±1.2	182.8±0.9
Inclination (°)	31.4±0.3	31.1±0.4
Longitude of ascending node (°)	213±2	210.3±1.2
Time of periastron (MJD)	60377.88±0.04	60377.85±0.02
Mass ratio (M_2/M_1)	$0.90^{+0.06}_{-0.02}$	$0.91^{+0.06}_{-0.05}$
Mass of Ba, M_1 (M_{Jup})	38.1±1.0	37±1
Mass of Bb, M_2 (M_{Jup})	34.4±1.5	34±1
Flux ratio, f_2/f_1 (2.0 μm)	0.47±0.03	0.53±0.02
γ_{RV} (km s^{-1})	0.4±0.2	0.46±0.20
Total mass of B (M_{Jup})	72.5±1.3	71.3±0.5

The argument of periastron refers to the primary brown dwarf, Gliese 229 Ba.

exact processes for dissipation is unclear, tidal interactions between the gaseous envelopes or accretion disks around the forming objects are probably important[33,34]. For binary brown dwarfs orbiting stars, fragmentation of a massive circumstellar disk is another potential formation route, in which two proto-brown dwarfs fragment in the disk and become bound in a close encounter[33]. Ultimately, any formation mechanism would need to account for the highly eccentric outer orbit of Gliese 229 A-Bab and the misalignments between the inner orbit, outer orbit and host star spin axis.

Thirty years after its discovery, Gliese 229 B continues to teach us about substellar objects. The discovery of Gliese 229 BaBb provides a potential resolution to the mass–luminosity tension for brown dwarf companions and suggests that other unusually massive brown dwarfs, such as HD 4113 C (ref. 2), could be unresolved substellar binaries as well. Future efforts to resolve other anomalous brown dwarf companions into binaries are essential for rigorously testing substellar evolutionary models, which are routinely used to interpret observations of giant planets. Although known binary brown dwarfs have separations peaking between 1 and 3 AU (ref. 16), Gliese 229 Bab demonstrates the existence of binary substellar companions to stars with separations well below 1 AU. The 12-day orbital period of Gliese 229 Bab places the two brown dwarfs deep within the Hill sphere of each other, suggesting a formation pathway that involves substantial energy dissipation. A main goal of exoplanet studies in the next decade is the search for exomoons and binary planets. Among isolated binary brown dwarfs, there are already examples of systems in which both components have masses in the planetary regime[35,36] (below 13 M_{Jup}), as well as several systems with roughly 4–13-M_{Jup} companions orbiting low-mass brown dwarfs[37–39]. It is unclear how common binary planets or exomoons are around stars. With further improvements in sensitivity, the combination of interferometry, high-resolution spectroscopy and transit photometry is poised to unveil new discoveries and provide insights into these questions.

Online content

Any methods, additional references, Nature Portfolio reporting summaries, source data, extended data, supplementary information, acknowledgements, peer review information; details of author contributions and competing interests; and statements of data and code availability are available at https://doi.org/10.1038/s41586-024-08064-x.

1. Brandt, M. et al. Improved dynamical masses for six brown dwarf companions using Hipparcos and Gaia EDR3. *Astron. J.* **162**, 301 (2021).
2. Cheetham, A. et al. Direct imaging of an ultracool substellar companion to the exoplanet host star HD 4113 A. *Astron. Astrophys.* **680**, A64 (2018).
3. Li, Y. et al. Surveying nearby brown dwarfs with HGCA: direct imaging discovery of a faint, high-mass brown dwarf orbiting HD 176535 A. *Mon. Not. R. Astron. Soc.* **522**, 5622–5637 (2023).
4. Howe, A. R., Mandell, A. M. & McElwain, M. W. Investigating possible binarity for GJ 229B. *Astrophys. J. Lett.* **951**, L25 (2023).
5. Nakajima, T. et al. Discovery of a cool brown dwarf. *Nature* **378**, 463–465 (1995).
6. Oppenheimer, B. R. et al. Infrared spectrum of the cool brown dwarf Gl 229B. *Science* **270**, 1478–1479 (1995).
7. Filippazzo, J. C. et al. Fundamental parameters and spectral energy distributions of young and field age objects with masses spanning the stellar to planetary regime. *Astrophys. J.* **810**, 158 (2015).
8. Saumon, D. & Marley, M. S. The evolution of L and T dwarfs in color-magnitude diagrams. *Astrophys. J.* **689**, 1327 (2008).
9. Phillips, M. W. et al. A new set of atmosphere and evolution models for cool T–Y brown dwarfs and giant exoplanets. *Astron. Astrophys.* **637**, A38 (2020).
10. Oppenheimer, B. R., Kulkarni, S. R., & Stauffer, J. R. in *Protostars and Planets IV* (eds Mannings, V. Boss, A. P. & Russell, S. S.) 1313 (Univ. Arizona Press, 2000).
11. Morley, C. V. et al. The Sonora substellar atmosphere models. III. Diamondback: atmospheric properties, spectra, and evolution for warm cloudy substellar objects. Preprint at https://arxiv.org/abs/2402.00758 (2024).
12. Burgasser, A. J., Geballe, T. R., Leggett, S. K., Kirkpatrick, J. D. & Golimowski, D. A. A unified near-infrared spectral classification scheme for T dwarfs. *Astrophys. J.* **637**, 1067 (2006).
13. Brandt, T. D. et al. A dynamical mass of 70 ± 5 M_{Jup} for Gliese 229B, the first T dwarf. *Astron. J.* **160**, 196 (2020).
14. Gaia Collaboration. Gaia Data Release 3. Summary of the content and survey properties. *Astron. Astrophys.* **674**, A1 (2023).
15. Burgasser, A. J. et al. in *Protostars and Planets V* (eds Reipurth, B. Jewitt, D. & Keil, K.) 427 (Univ. Arizona Press, 2007).
16. Fontanive, C., Biller, B., Bonavita, M. & Allers, K. Constraining the multiplicity statistics of the coolest brown dwarfs: binary fraction continues to decrease with spectral type. *Mon. Not. R. Astron. Soc.* **479**, 2702–2727 (2018).
17. GRAVITY+ Collaboration et al. First light for GRAVITY Wide. Large separation fringe tracking for the Very Large Telescope Interferometer. *Astron. Astrophys.* **665**, A75 (2022).
18. Dorn, R. J. et al. CRIRES+ on sky at the ESO Very Large Telescope. Observing the Universe at infrared wavelengths and high spectral resolution. *Astron. Astrophys.* **671**, A24 (2023).
19. Gallenne, A. et al. Robust high-contrast companion detection from interferometric observations. The CANDID algorithm and an application to six binary Cepheids. *Astron. Astrophys.* **579**, A68 (2015).
20. Mukherjee, S. et al. The Sonora substellar atmosphere models. IV. Elf Owl: atmospheric mixing and chemical disequilibrium with varying metallicity and C/O ratios. *Astrophys. J.* **963**, 73 (2024).
21. Calamari, E. et al. An atmospheric retrieval of the brown dwarf Gliese 229B. *Astrophys. J.* **940**, 164 (2022).
22. Mérand, A. Flexible spectro-interferometric modelling of OIFITS data with PMOIRED. *Proc. SPIE* **12183**, 121831N (2022).
23. Thompson, W. et al. Octofitter: fast, flexible, and accurate orbit modeling to detect exoplanets. *Astron. J.* **166**, 164 (2023).
24. Dupuy, T. J. & Liu, M. C. Individual dynamical masses of ultracool dwarfs. *Astrophys. J. Suppl. Ser.* **231**, 15 (2017).
25. Bowler, B. P. et al. Rotation periods, inclinations, and obliquities of cool stars hosting directly imaged substellar companions: spin–orbit misalignments are common. *Astron. J.* **165**, 164 (2023).
26. Chabrier, G., Baraffe, I., Phillips, M. & Debras, F. Impact of a new H/He equation of state on the evolution of massive brown dwarfs. New determination of the hydrogen burning limit. *Astron. Astrophys.* **671**, A119 (2023).
27. Hsu, C.-C., Burgasser, A. J. & Theissen, C. A. Discovery of the exceptionally short period ultracool dwarf binary LP 413-53AB. *Astrophys. J. Lett.* **945**, L6 (2023).
28. Lodieu, N. et al. An eclipsing double-line spectroscopic binary at the stellar/substellar boundary in the Upper Scorpius OB association. *Astron. Astrophys.* **584**, A128 (2015).
29. Stassun, K. G., Mathieu, R. D. & Valenti, J. A. Discovery of two young brown dwarfs in an eclipsing binary system. *Nature* **440**, 311–314 (2006).
30. Triaud, A. H. M. J. et al. An eclipsing substellar binary in a young triple system discovered by SPECULOOS. *Nat. Astron.* **4**, 650–657 (2020).
31. Low, C. & Lynden-Bell, D. The minimum Jeans mass or when fragmentation must stop. *Mon. Not. R. Astron. Soc.* **176**, 367–390 (1976).
32. Burgasser, A. J. et al. Discovery of a very low mass triple with late-M and T dwarf components: LP 704-48/SDSS J0006-0852AB. *Astrophys. J.* **757**, 110 (2012).
33. Stamatellos, D. & Whitworth, A. P. The properties of brown dwarfs and low-mass hydrogen-burning stars formed by disc fragmentation. *Mon. Not. R. Astron. Soc.* **392**, 413–427 (2009).
34. Lazzoni, C., Rice, K., Zurlo, A., Hinkley, S. & Desidera, S. Binary planet formation through tides. *Mon. Not. R. Astron. Soc.* **527**, 3837–3846 (2024).
35. Best, W. M. J., Liu, M. C., Dupuy, T. J. & Magnier, E. A. The young L dwarf 2MASS J11193254–1137466 is a planetary-mass binary. *Astrophys. J. Lett.* **843**, L4 (2017).
36. Theissen, C. A. et al. WISE J135501.90-825838.9 is a nearby, young, extremely low-mass substellar binary. *Res. Notes AAS* **4**, 67 (2020).
37. Bowler, B. P. & Hillenbrand, L. A. Near-infrared spectroscopy of 2M0441+2301 AabBab: a quadruple system spanning the stellar to planetary mass regimes. *Astrophys. J. Lett.* **811**, L30 (2015).
38. Chauvin, G. et al. A giant planet candidate near a young brown dwarf. Direct VLT/NACO observations using IR wavefront sensing. *Astron. Astrophys.* **425**, L29 (2004).
39. Calissendorff, P. et al. JWST/NIRCam discovery of the first Y+Y brown dwarf binary: WISE J033605.05-014350.4. *Astrophys. J. Lett.* **947**, L30 (2023).

Publisher's note Springer Nature remains neutral with regard to jurisdictional claims in published maps and institutional affiliations.

[1]Department of Astronomy, California Institute of Technology, Pasadena, CA, USA. [2]European Southern Observatory, Garching, Germany. [3]Department of Physics and Astronomy, University of Victoria, Victoria, British Columbia, Canada. [4]LESIA, Observatoire de Paris, Université PSL, CNRS, Sorbonne Université, Université Paris Cité, Meudon, France. [5]National Research Council of Canada Herzberg, Victoria, British Columbia, Canada. [6]Jet Propulsion Laboratory, California Institute of Technology, Pasadena, CA, USA. [7]Department of Astrophysics, American Museum of Natural History, New York, NY, USA. [8]Division of Geological and Planetary Sciences, California Institute of Technology, Pasadena, CA, USA. [9]Center for Interdisciplinary Exploration and Research in Astrophysics (CIERA), Northwestern University, Evanston, IL, USA. [10]Department of Physics and Astronomy, Northwestern University, Evanston, IL, USA. [11]Center for Astrophysics and Space Sciences, University of California, San Diego, La Jolla, CA, USA. [12]Institute for Astronomy, University of Hawai'i, Honolulu, HI, USA. [13]Max-Planck-Institut für Astronomie, Heidelberg, Germany. [14]European Space Agency (ESA), ESA Office, Space Telescope Science Institute, Baltimore, MD, USA. [15]Department of Astronomy and Astrophysics, University of California, Santa Cruz, Santa Cruz, CA, USA. [16]Department of Physics & Astronomy, Johns Hopkins University, Baltimore, MD, USA. [17]Max Planck Institute for Extraterrestrial Physics, Garching, Germany. [18]Laboratoire Lagrange, Observatoire de la Côte d'Azur, Université Côte d'Azur, CNRS, Nice, France. [19]1st Institute of Physics, University of Cologne, Cologne, Germany. [20]Max Planck Institute for Radio Astronomy, Bonn, Germany. [21]Faculdade de Engenharia, Universidade do Porto, Porto, Portugal. [22]Centro de Astrofísica e Gravitação (CENTRA), Instituto Superior Técnico (IST), Universidade de Lisboa, Lisboa, Portugal. [23]Physics Building, University of Exeter, Exeter, United Kingdom. [24]School of Physics and Astronomy, University of Southampton, Southampton, United Kingdom. [25]Department of Astronomy, Stockholm University, Stockholm, Sweden. [26]Université Grenoble Alpes, CNRS, IPAG, Grenoble, France. [27]Fakultät für Physik, Universität Duisburg-Essen, Duisburg, Germany. [28]Institut für Astronomie und Astrophysik, Universität Tübingen, Tübingen, Germany. [29]Physikalisches Institut, Universität Bern, Bern, Switzerland. [30]Institute of Astronomy, University of Cambridge, Cambridge, United Kingdom. [31]Institute of Astronomy and Astrophysics, Academia Sinica, Taipei, Taiwan. [32]Leiden Observatory, Leiden University, Leiden, The Netherlands. [33]Aix-Marseille Université, CNRS, CNES, LAM, Marseille, France. [34]These authors contributed equally: A. Mérand, W. Thompson. ✉e-mail: wxuan@caltech.edu

Methods

VLTI/GRAVITY observations and data reduction

We observed Gliese 229 BaBb with GRAVITY[40] at the VLTI using the four Unit Telescopes at Cerro Paranal (programme IDs: 0112.C-2369(A) and 2112.D-5036(A); PI: Xuan). We obtained data at five epochs: 26 and 30 December 2023, 28 February 2024, 29 March 2024 and 29 April 2024 UT (universal time). We used GRAVITY in the wide-angle dual-field mode[17], recently commissioned as part of the GRAVITY+ upgrade[41]. In this mode, the field is divided into two at the telescope level and carried independently within the GRAVITY delay lines. One field, centred on the star Gliese 229 A, is used by the GRAVITY fringe tracker[42,43] to stabilize the fringes by compensating for the atmospheric piston and vibrations in the system. The other field, centred on the companion (now known to be binary), is observed by the GRAVITY spectrometer. The scientific observations were conducted with medium spectral resolution (R = 500) in the unpolarized mode. A log of the observations is given in Extended Data Table 1.

The reduction of the raw data was performed using the ESO GRAVITY pipeline v1.6.4 (ref. 44). This version of the pipeline can reduce the wide-angle data, but we had to disable the acquisition camera reduction to do so. In wide-angle mode, we could not use the fringe tracker to reference the phase (as is traditionally done for exoplanet observations; see ref. 45), but we could use the closure phase to detect the companion. The closure phases are averaged for each exposure, yielding several values per night.

The best datasets were obtained during the first two nights (see Extended Data Table 1). In December 2023, the two epochs showed closure phase values on the order of 40° between 2.0 and 2.2 µm, with a signal-to-noise ratio (S/N) greater than 10. At longer wavelengths, CH_4 absorption and lower instrumental throughout prevent us from recording a robust closure phase. The closure phase signal was clear enough to confirm the binary nature of Gliese 229 BaBb. Moreover, injection-recovery tests show that the first epoch GRAVITY data are sensitive to objects 2–3 magnitudes fainter than Gliese 229 Ba at separations from 3 to 19 mas, largely ruling out a third brown dwarf in the field. Although the binary detection was clear, the data were too sparse to determine the orbital parameters, so we requested ESO Director's Discretionary Time to continue monitoring the object from February to late April, after which the target was no longer observable. The data quality was poor in February owing to seeing conditions and in March owing to an issue with the pointing of the GRAVITY fibres. Despite this, a few below-average-quality datasets were salvageable. The last dataset, obtained on 29 April 2024 UT, was of high quality, benefiting from a recent instrumental upgrade of the VLTI beam compressor differential delay lines. During this last run, a S/N close to 20 was achieved, providing a clear detection to finalize the astrometric orbit of the binary.

VLT/CRIRES+ observations and data reduction

We observed the Gliese 229 system with the upgraded CRIRES+ (refs. 18,46) mounted on the Very Large Telescope (programme ID: 0112.C-2369(B); PI: Xuan). We obtained seven epochs of data on 19 and 20 February 2024, 1, 19 and 20 March 2024 and 7 and 8 April 2024 UT (see log in Extended Data Table 1). The wavelength setting H1567 and 0.2 arcsec slit width were used to cover H_2O and CH_4 absorption lines from 1.47 to 1.78 µm and achieve a spectral resolution of $R \approx 100{,}000$. The observations were taken in adaptive optics mode. For each epoch, we first observe the A0V telluric standard star 10 Lep (which is at a similar air mass as Gliese 229) and the primary star Gliese 229 A, before offsetting the slit to the location of the companion approximately 4.4 arcsec away. The relative astrometry of the companion is determined using the orbit from ref. 1. The CRIRES+ slit was set perpendicular to the position angle of the companion to minimize the leakage of starlight into the slit. We used the standard ABBA nodding scheme for background removal.

We reduced the data with a customized open-source pipeline excalibuhr[47]. It follows the general calibration steps of the ESO's CR2RES pipeline, including dark and flat correction, spectral order tracing, slit curvature tracing and initial wavelength solution. We removed the sky background by means of nod subtraction and combined individual exposures at each nodding position. The 1D spectra were then extracted using the optimal extraction method[48]. We used the spectrum of the standard star 10 Lep as a proxy to remove the telluric transmission features. The wavelength regions contaminated by strong telluric lines (with transmission less than 70%) were masked in the following analyses. Using observations of the telluric standard star, we carried out an extra wavelength calibration against a telluric transmission model generated by the ESO's sky model calculator SkyCalc[49,50]. This was achieved by applying a third-order polynomial to the initial wavelength solution in each order and optimizing the correlation between the observed spectrum of the telluric standard star and the template spectrum.

On average, we achieved a S/N ≈ 30 per wavelength channel per epoch at 1.57 µm for the extracted spectra of Gliese 229 BaBb, which includes emission from the companion and stellar contamination at the location of the companion. To estimate the spectral resolution of our observations, we used the ESO sky software Molecfit[51] to fit the spectra of the telluric standard star. We find stable line spread functions across different nights with Gaussian profile widths of 3.05, 3.12, 3.28, 3.27, 3.05, 3.28 and 3.05 pixels for the seven epochs, respectively. They correspond to an average resolving power of roughly 100,000, as expected.

Extraction of RVs from CRIRES+

To calculate the RVs of Gliese 229 Ba and Bb, we fit the CRIRES+ spectrum from 1.510 to 1.583 µm, which covers two spectral orders. Each order is broken up into three chunks that are recorded on different detectors. The data from 1.45 to 1.50 µm are omitted owing to substantial telluric contamination. We also omit the data longward of 1.60 µm for two reasons. First, Gliese 229 Ba and Bb are extremely faint from 1.6 to 1.78 µm as a result of CH_4 absorption (see low-resolution spectrum in ref. 52), which results in lower S/N data. Second, our preliminary fits show that the models provide a poorer match to the data beyond 1.6 µm. Although we are using the most accurate CH_4 line list from ref. 53, ref. 54 showed that even this line list can produce discrepant $v\sin i$, RV and T_{eff} measurements by fitting the spectrum of an isolated T dwarf. To avoid biasing the RV measurements, we focus on the water-dominated region from 1.510 to 1.583 µm, at which the H_2O line list from ref. 55 is shown to be accurate[54].

In the spectrum of Gliese 229 BaBb, we noticed atomic lines from Gliese 229 A, indicating a modest amount of stellar contamination from the bright host star (ten magnitudes brighter in the H band). Therefore, we model the spectrum of Gliese 229 BaBb with three components: two brown dwarfs (Ba and Bb) and the primary star. The models for the brown dwarfs are generated using the temperature and abundances profiles from Sonora Elf Owl[20]. As the resolution limit of Elf Owl is R = 5,000, we recompute the models at R = 1,000,000 using the open-source radiative transfer code petitRADTRANS[56]. We include the line opacities of CH_4, H_2O, CO, CO_2, H_2S, NH_3, PH_3, C_2H_2, HCN, Na, K and FeH, as well as H_2–H_2 and H_2–He continuum opacities. To account for stellar contamination, we use the CRIRES+ spectrum of the star taken immediately before the Gliese 229 B exposures. Before fitting, we continuum-normalize each order of the Gliese 229 BaBb spectrum with a median filter of width 100 pixels (≈5 Å).

We fit the RV shift of the brown dwarfs at each observing date, the $v\sin i$ for each brown dwarf, flux scaling factors and multiplicative error inflation terms. A different flux scaling factor is used for Gliese 229 Ba and Bb and the primary star. To reduce the dimensionality, we optimize the linear flux scaling terms and error inflation terms at each iteration following ref. 57. In the fit, we rotationally broaden the atmospheric models using the code from ref. 58, apply the RV shifts and convolve the models to R = 100,000 with a Gaussian profile. Next, we apply the optimal scale factors to the respective models to construct the combined model (Fig. 2a) and apply the same median filter to the combined model. The posterior is sampled with the nested sampling code DYNESTY[59] and we use 1,000 live points. We find that, on average, the host star contributes about 20% of the total flux in the Gliese 229 BaBb spectrum. Because the lines from the M1V primary star are very distinct from T dwarf lines (for example, Fig. 1), they do not affect our RV measurements.

After obtaining the RV posteriors, we apply barycentric corrections for each night using tools in the Astropy package[60] and subtract the RV of the primary star taken from ref. 61. The resulting RV points of Gliese 229 Ba and Bb are shown in Fig. 2b and included in Extended Data Table 3. The statistical errors on the measured RVs are typically about 0.1 km s^{-1}. We consider several sources of systematic uncertainties. First, we measure the stellar RVs over the same nights to assess the instrumental jitter. The procedure is described below and adds an uncertainty of 0.1 km s^{-1}. Second, we consider the impact that uncertain atmospheric parameters have on the retrieved RVs by repeating the spectral fits with a range of different models. Apart from the fiducial model (850 K + 750 K), we consider the following $T_{\rm eff}$ combinations: (900 K + 800 K), (900 K + 750 K), (850 K + 700 K), (850 K + 800 K) and (800 K + 750 K). We set log(g) = 5.0, C/O = 0.68 and [M/H] = 0.0 for all models. The abundances are chosen to match those of the host star, which has a nearly solar metallicity[62,63] and C/O = 0.68 ± 0.12 (ref. 64). The log(g) is fixed because the evolutionary models predict a relatively small range of variation in log(g) (see Extended Data Table 2). Also, we fix the vertical eddy diffusion parameter log(K_{zz}) to 2.0, as found by ref. 20. We use the scatter in RV values derived from each fit as an independent source of systematic error. These add systematic uncertainties on the order of approximately 0.2–0.7 km s^{-1}, depending on the epoch.

We compute CCFs of the primary star spectra to verify the stability of the CRIRES+ wavelength solution and line spread function (Extended Data Fig. 3). We adopt a PHOENIX-ACES model[65] with $T_{\rm eff}$ = 3,800 K and log(g) = 4.5 for the primary star. Over the 2.5-month observing period, the RV change caused by orbital motion of Gliese 229 A around the system barycentre is <2 m s^{-1}, which we ignore. Approximating the stellar CCFs as Gaussian functions, we measure the stellar RVs as the centre of the Gaussian. We find that the stellar RV is stable at the 0.1 km s^{-1} level across the seven observing epochs.

From the CRIRES+ fits, we find that the two brown dwarfs have projected rotation rates ($v$sin$i$) below our measurement limit. The 3σ upper limits of $v$sin$i$ for Gliese 229 Ba and Bb are <0.6 and <0.7 km s^{-1}, respectively. If the two brown dwarfs are tidally synchronized, their rotational velocities would be about 0.4 km s^{-1}. Assuming that their rotational axes are aligned with the orbital axis, this implies $v$sin$i$ ≈ 0.2 km s^{-1}, which is well below the size of the line spread function (≈3 km s^{-1}) for CRIRES+. Thus, our non-detection of spin is consistent with the brown dwarfs being tidally locked, or nearly tidally locked, which is expected on the basis of their tidal despinning time (see the 'Dynamics' section).

Bulk properties of Gliese 229 Ba and Bb

Using ATMO 2020 evolutionary models[9], we estimate the component masses of Gliese 229 Ba and Bb that best reproduce the bolometric luminosity of log($L/L_\odot$) of −5.21 ± 0.05 (ref. 7) and GRAVITY K band flux ratio of 0.47 ± 0.03. We also include J, H and K magnitudes of the combined source[66] as constraints in our fit. ATMO 2020 includes three separate models with differing amounts of non-equilibrium (NEQ) chemistry. We adopt the 'NEQ weak' model but note that the results are similar if we used 'NEQ strong' or 'CEQ'. We use ATMO 2020 tables with precomputed Mauna Kea Observatories (MKO) magnitudes. Although the GRAVITY K band transmission profile is not identical to that of MKO K, the flux ratio measurement effectively divides out the transmission function. Our fit is parameterized with three parameters: mass ratio, age and total mass. We place a Gaussian prior of 72.5 ± 1.3 $M_{\rm Jup}$ on total mass, as derived from our orbit fit. For a given set of masses and age, we interpolate to obtain the log($L/L_\odot$) and J, H and K magnitude of each brown dwarf, requiring that their combined magnitudes and luminosities match the observed values. We sample the posterior using a Markov chain Monte Carlo method[67] with 10,000 steps and 30 walkers. The first 2,000 steps are discarded as burn-in. Overall, the ATMO 2020 models match the observations well for an age of 2.45 ± 0.2 Gyr (Fig. 3). The inferred age is model-dependent, but we find that ages of 2–4 Gyr generally match the properties of the binary brown dwarf by considering alternative evolutionary models in Extended Data Fig. 1.

From the ATMO 2020 model, we also interpolate for the $T_{\rm eff}$, log(g) and log($L/L_\odot$) of each brown dwarf, which we tabulate in Extended Data Table 2. We adopt the closest grid points in Sonora Elf Owl to these values to compute high-resolution spectral models and fit the CRIRES+ spectra. We emphasize that these $T_{\rm eff}$ estimates are model-based. Upcoming James Webb Space Telescope spectroscopy of Gliese 229 BaBb from 1 to 15 μm (GO3762; PI: Xuan) should enable robust two-component spectral fits and provide independent estimates of the bulk properties for each brown dwarf.

We perform a second estimate of the bulk properties of Gliese 229 Ba and Bb using calibrated empirical relations for field brown dwarfs from ref. 68. First, we estimate individual absolute MKO $M_{\rm K}$ magnitudes of Gliese 229 Ba and Bb from their combined-light MKO K magnitude ($K_{\rm MKO}$ = 14.36 ± 0.05)[66], the GRAVITY K band flux ratio (0.47 ± 0.03) and the system parallax (173.574 ± 0.017 mas)[14]. This yields $M_{\rm K,Ba}$ = 15.98 ± 0.05 mag and $M_{\rm K,Bb}$ = 16.80 ± 0.05 mag. Next, using the MKO $M_{\rm K}$–$L_{\rm bol}$ and MKO $M_{\rm K}$–$T_{\rm eff}$ relations for field objects in ref. 68, we find log($L/L_\odot$), Ba = −5.36 ± 0.07 dex, $T_{\rm eff,Ba}$ = 810 ± 55 K and log($L/L_\odot$), Bb = −5.56 ± 0.07 dex, $T_{\rm eff,Bb}$ = 694 ± 55 K. These values are consistent with those inferred from the ATMO 2020 evolutionary models at the approximately 1σ level. The closest matching spectral types are T7 for Gliese 229 Ba and T8 for Gliese 229 Bb.

Orbit fits

To derive orbital parameters, we jointly fit the GRAVITY closure phases and CRIRES+ RVs. Instead of computing positions from the closure phases for each epoch, we directly model them in the orbit fit. Not only does this take into account the numerous possible positions at each epoch but it also avoids intermediate products, preserving noise properties. We implemented this joint model in two different frameworks: a frequentist approach in PMOIRED[22] and a Bayesian approach in Octofitter[23]. These methods independently arrive at consistent results. The methods were also validated using high-quality GRAVITY data and high-S/N RVs from VLT/UVES[69] for a binary star system, for which we confirm that a closure-phase orbital fit and an orbit fit using per-epoch separations and position angles yielded the same result. In both codes, we adopt a standard coordinate system for the orbit in which +X points east, +Y points north and +Z points away from the observer.

For the PMOIRED analysis, the best orbit is found by gradient descent, first on the RV data and then on the joint model after adding the closure phase data. We only include the GRAVITY data from 2.05 to 2.18 μm, as strong methane absorption results in extremely low S/N past 2.18 μm. Also, the wavelength channels are binned to six points over the 2.05–2.18-μm range. To better estimate the final uncertainties, bootstrapping is used: 5,000 random datasets are generated using sampling with replacement, and each time an orbital solution is fitted from a first guess drawn around the best values with four times the uncertainties. Bootstrapping has been shown to mitigate the correlations in interferometric data analysis[70]. GRAVITY data are correlated, primarily because closure phases share baselines and baselines share telescopes (as formalized in ref. 71). Moreover, data taken at the same time and with the same telescope triples have experienced the same biases from atmospheric turbulence and same calibration processes. To account for these correlations, all closure phases from the same date and baseline triangle are drawn together in the bootstrapping. First, we search for the best-fit orbit to the RV data alone. This leads to an excellent solution with $P = 12.12 \pm 0.04$ days, $e = 0.22 \pm 0.03$, $q = 0.91 \pm 0.03$ and a reduced χ^2 of 1.3. We allow for a RV offset term, γ_{RV} to account for possible inaccuracies in the systematic RV of the system. Next, we perform a joint fit to the GRAVITY and CRIRES+ data. The results are shown in Table 1 and the relative orbit of the binary brown dwarf is plotted in Extended Data Fig. 6. We adopt the PMOIRED results as the baseline values in this paper.

For the Octofitter analysis, we completed joint Bayesian modelling of both the CRIRES+ RVs and GRAVITY data. We used non-reversible parallel tempering[72–75] to search the entire multimodal parameter space globally for the best-fitting parameter values. Rather than working with the closure phases directly, this analysis first converts the closure phases into a set of non-redundant kernel phases for each wavelength[76]. This improves the accuracy of the model uncertainties compared with working directly with the closure phases, which share baselines (mitigated in the PMOIRED analysis after the fact using bootstrapping). Finally, we add an extra kernel-phase 'jitter' term for each epoch of data (five in total). This term allows the model to absorb some amount of systematic calibration error in the GRAVITY data, again resulting in more realistic uncertainties in the final model parameters. For this model, we included data in the 2.025–2.150-μm range with no spectral binning. The orbital parameters from the joint model are listed in Table 1 and are consistent with PMOIRED results at the approximately 1.5σ level. We find strong evidence that, when combining the GRAVITY data with the CRIRES+ RVs, the orbit solution is uniquely determined and no secondary modes in the posterior are notable.

We provide posterior predictions of the relative separation and position angle of Gliese 229 Ba-Bb in Extended Data Table 4. We stress that these are inferred values and not statistically independent, such as in traditional astrometry, as they are derived from a joint analysis of all epochs. They should not be used as inputs to an orbit fit, as they themselves are the outputs of such a fit. Instead, orbit fits should use the GRAVITY closure phases.

Dynamics

Given their small separation, Gliese 229 Ba and Bb are probably tidally locked with each other, with rotation periods equal to the orbital period of 12 days. We quantify the tidal locking timescale using ref. 77. With an initial spin velocity of 20 km s^{-1} and initial radius of 1 $R_{\rm Jup}$, we find a despinning time of about 2 Gyr, which is shorter than or comparable with the estimated system age of approximately 2–6 Gyr (ref. 13). As noted earlier, our CRIRES+ analysis shows that both brown dwarfs have $v\sin i < 0.7$ km s^{-1}, which is consistent with them being tidally locked.

In the current configuration of Gliese 229 A-BaBb, the highly eccentric and misaligned outer AB orbit ($e \approx 0.85$)[1] could induce secular perturbations that pump up the eccentricity of the inner BaBb orbit by means of the eccentric von Zeipel–Lidov–Kozai mechanism[78]. Consequently, tidal interactions may shrink the BaBb orbit. We estimate that the Kozai secular precession timescale given by equation (3) in ref. 79 is about 0.2 Myr for Gliese 229 Bb. The secondary brown dwarf also undergoes precession from the quadrupole potential from its tidal and rotational bulges and from the leading order effects of general relativity. If these effects operate on a shorter timescale, they could suppress Kozai oscillations. For our brown dwarfs, we adopt tidal parameters $Q = 3 \times 10^4$, $k_2 = 0.565$ based on Jupiter. The exact values of Q and k_2 are unknown for brown dwarfs but estimates from hot Jupiters generally produce values within one order of magnitude of Jupiter's values[80]. We estimate the precession rates using equations (6)–(8) in ref. 79 and find that the precession rate owing to general relativity is the fastest, with a corresponding timescale of about 0.6 Myr, which is still longer than the Kozai timescale. In the absence of further perturbations or bodies, the triple system may therefore undergo Kozai oscillations. However, detailed N-body simulations and follow-up work are required to further evaluate the dynamical state of the system.

Data availability

The reduced CRIRES+ and GRAVITY data will be made public through Zenodo[81] at: https://doi.org/10.5281/zenodo.13851639.

Code availability

The CRIRES+ data reduction was performed with excalibuhr (https://github.com/yapenzhang/excalibuhr). The orbit fits were performed with PMOIRED (https://github.com/amerand/PMOIRED) and Octofitter (https://sefffal.github.io/Octofitter.jl/dev/). The atmospheric models were generated using inputs from Sonora Elf Owl (https://zenodo.org/records/10385821) and the petitRADTRANS radiative transfer tool available at https://petitradtrans.readthedocs.io/. ATMO 2020 models are available for download at http://opendata.erc-atmo.eu.

40. GRAVITY Collaboration et al. First light for GRAVITY: phase referencing optical interferometry for the Very Large Telescope Interferometer. *Astron. Astrophys.* **602**, A94 (2017).
41. Eisenhauer, F. GRAVITY+: towards faint science. The Very Large Telescope in 2030 (VLT2030). *Zenodo* https://doi.org/10.5281/zenodo.3356274 (2019).
42. Lacour, S. et al. The GRAVITY fringe tracker. *Astron. Astrophys.* **624**, A99 (2019).
43. Nowak, M. et al. Upgrading the GRAVITY fringe tracker for GRAVITY+. Tracking the white-light fringe in the non-observable optical path length state-space. *Astron. Astrophys.* **684**, A184 (2024).
44. Lapeyrere, V. et al. GRAVITY data reduction software. *Proc. SPIE* **9146**, 91462D (2014).
45. Lacour, S., Carrión-González, Ó., & Nowak, M. Exoplanets in reflected starlight with dual-field interferometry: a case for shorter wavelengths and a fifth Unit Telescope at VLTI/Paranal. Preprint at https://arxiv.org/abs/2406.07030 (2024).
46. Dorn, R. J. et al. CRIRES+: exploring the cold universe at high spectral resolution. *The Messenger* **156**, 7–11 (2014).
47. Zhang, Y. excalibuhr. *GitHub* https://github.com/yapenzhang/excalibuhr (2024)
48. Horne, K. An optimal extraction algorithm for CCD spectroscopy. *Publ. Astron. Soc. Pac.* **98**, 609 (1986).
49. Noll, S. et al. An atmospheric radiation model for Cerro Paranal. I. The optical spectral range. *Astron. Astrophys.* **543**, A92 (2012).
50. Jones, A., Noll, S., Kausch, W., Szyszka, C. & Kimeswenger, S. An advanced scattered moonlight model for Cerro Paranal. *Astron. Astrophys.* **560**, A91 (2013).
51. Smette, A. et al. Molecfit: a general tool for telluric absorption correction. *Astron. Astrophys.* **576**, A77 (2015).
52. Geballe, T. R., Kulkarni, S. R., Woodward, C. E. & Sloan, G. C. The near-infrared spectrum of the brown dwarf Gliese 229B. *Astrophys. J. Lett.* **467**, L101 (1996).
53. Hargreaves, R. J. et al. An accurate, extensive, and practical line list of methane for the HITEMP database. *Astrophys. J. Suppl. Ser.* **247**, 55 (2020).
54. Tannock, M. E. et al. A 1.46–2.48 μm spectroscopic atlas of a T6 dwarf (1060 K) atmosphere with IGRINS: first detections of H_2S and H_2, and verification of H_2O, CH_4, and NH_3 line lists. *Mon. Not. R. Astron. Soc.* **514**, 3160–3178 (2022).
55. Polyansky, O. L. et al. ExoMol molecular line lists XXX: a complete high-accuracy line list for water. *Mon. Not. R. Astron. Soc.* **480**, 2597–2608 (2018).
56. Mollière, P. et al. petitRADTRANS. A Python radiative transfer package for exoplanet characterization and retrieval. *Astron. Astrophys.* **627**, A67 (2019).
57. Ruffio, J.-B. et al. Detecting exomoons from radial velocity measurements of self-luminous planets: application to observations of HR 7672 B and future prospects. *Astron. J.* **165**, 113 (2023).
58. Carvalho, A. & Johns-Krull, C. M. A simple code for rotational broadening of broad wavelength range high-dispersion spectra. *Res. Notes AAS* **7**, 91 (2023).
59. Speagle, J. S. DYNESTY: a dynamic nested sampling package for estimating Bayesian posteriors and evidences. *Mon. Not. R. Astron. Soc.* **493**, 3132–3158 (2020).
60. Astropy Collaboration et al. The Astropy Project: sustaining and growing a community-oriented open-source project and the latest major release (v5.0) of the core package. *Astrophys. J.* **935**, 167 (2022).
61. Fouqué, P. et al. SPIRou Input Catalogue: global properties of 440 M dwarfs observed with ESPaDOnS at CFHT. *Mon. Not. R. Astron. Soc.* **475**, 1960–1986 (2018).
62. Neves, V. et al. Metallicity of M dwarfs. III. Planet-metallicity and planet-stellar mass correlations of the HARPS GTO M dwarf sample. *Astron. Astrophys.* **551**, A36 (2013).
63. Kuznetsov, M. K., del Burgo, C., Pavlenko, Y. V. & Frith, J. Characterization of a sample of southern M dwarfs using HARPS and X-shooter spectra. *Astrophys. J.* **878**, 134 (2019).
64. Nakajima, T., Tsuji, T. & Takeda, Y. Physical properties of Gliese 229B based on newly determined carbon and oxygen abundances of Gliese 229A. *Astron. J.* **150**, 53 (2015).
65. Husser, T.-O. et al. A new extensive library of PHOENIX stellar atmospheres and synthetic spectra. *Astron. Astrophys.* **553**, A6 (2013).
66. Leggett, S. K. et al. Infrared photometry of late-M, L, and T dwarfs. *Astrophys. J.* **564**, 452 (2002).
67. Foreman-Mackey, D., Hogg, D. W., Lang, D. & Goodman, J. emcee: the MCMC hammer. *Publ. Astron. Soc. Pac.* **125**, 306 (2013).
68. Sanghi, A. et al. The Hawaii Infrared Parallax Program. VI. The fundamental properties of 1000+ ultracool dwarfs and planetary-mass objects using optical to mid-infrared spectral energy distributions and comparison to BT-Settl and ATMO 2020 model atmospheres. *Astrophys. J.* **959**, 63 (2023).

69. Gallenne, A. et al. The Araucaria project: high-precision orbital parallaxes and masses of binary stars. I. VLTI/GRAVITY observations of ten double-lined spectroscopic binaries. *Astron. Astrophys.* **672**, A119 (2023).
70. Lachaume, R. et al. Towards reliable uncertainties in IR interferometry: the bootstrap for correlated statistical and systematic errors. *Mon. Not. R. Astron. Soc.* **484**, 2656–2673 (2019).
71. Kammerer, J., Mérand, A., Ireland, M. J. & Lacour, S. Increasing the achievable contrast of infrared interferometry with an error correlation model. *Astron. Astrophys.* **644**, A110 (2020).
72. Syed, S., Bouchard-Côté, A., Deligiannidis, G. & Doucet, A. Non-reversible parallel tempering: a scalable highly parallel MCMC scheme. *J. R. Stat. Soc. B Stat. Methodol.* **84**, 321–350 (2022).
73. Surjanovic, N. et al. Pigeons.jl: distributed sampling from intractable distributions. Preprint at https://arxiv.org/abs/2308.09769 (2023).
74. Biron-Lattes, M., Surjanovic, N., Syed, S., Campbell, T. & Bouchard-Cote, A. in *Proc. 27th International Conference on Artificial Intelligence and Statistics* 4600–4608 (MLR Press, 2024).
75. Surjanovic, N., Syed, S., Bouchard-Côté, A. & Campbell, T. Parallel tempering with a variational reference. In *Advances in Neural Information Processing Systems NeurIPS 35* 565–577 (Curran Associates, Inc., 2022).
76. Blackburn, L. et al. Closure statistics in interferometric data. *Astrophys. J.* **894**, 31 (2020).
77. Peale, S. J. in *Planetary Satellites* (ed. Burns, J. A.) 87–111 (Univ. Arizona Press, 1977).
78. Naoz, S. The eccentric Kozai-Lidov effect and its applications. *Annu. Rev. Astron. Astrophys.* **54**, 441–489 (2016).
79. Batygin, K., Bodenheimer, P. & Laughlin, G. Determination of the interior structure of transiting planets in multiple-planet systems. *Astrophys. J. Lett.* **704**, L49 (2009).
80. Efroimsky, M. & Makarov, V. V. Tidal quality of the hot Jupiter WASP-12b. *Universe* **8**, 211 (2022).
81. Xuan, J., Thompson, W., Lacour, S., Blakely, D. & Mérand, A. GRAVITY and CRIRES+ data for Gliese 229Bab *Zenodo* https://doi.org/10.5281/zenodo.13851639 (2024).
82. Dupuy, T. J. & Liu, M. C. The Hawaii Infrared Parallax Program. I. Ultracool binaries and the L/T transition. *Astrophys. J. Suppl. Ser.* **201**, 19 (2012).
83. Dupuy, T. J. & Kraus, A. L. Distances, luminosities, and temperatures of the coldest known substellar objects. *Science* **341**, 1492–1495 (2013).
84. Deacon, N. R. et al. Wide cool and ultracool companions to nearby stars from Pan-STARRS 1. *Astrophys. J.* **792**, 119 (2014).
85. Liu, M. C., Dupuy, T. J. & Allers, K. N. The Hawaii Infrared Parallax Program. II. Young ultracool field dwarfs. *Astrophys. J.* **833**, 96 (2016).
86. Best, W. M. J. et al. Photometry and proper motions of M, L, and T dwarfs from the Pan-STARRS1 3π survey. *Astrophys. J. Suppl. Ser.* **234**, 1 (2018).
87. Best, W. M. J., Liu, M. C., Magnier, E. A. & Dupuy, T. J. A volume-limited sample of ultracool dwarfs. I. Construction, space density, and a gap in the L/T transition. *Astron. J.* **161**, 42 (2021).
88. Schneider, A. C. et al. Astrometry and photometry for ≈1000 L, T, and Y dwarfs from the UKIRT Hemisphere Survey. *Astron. J.* **166**, 103 (2023).
89. Allard, F., Hauschildt, P. H., Alexander, D. R., Tamanai, A. & Schweitzer, A. The limiting effects of dust in brown dwarf model atmospheres. *Astrophys. J.* **556**, 357 (2001).
90. Golimowski, D. A. et al. The Solar neighborhood. IX. Hubble Space Telescope detections of companions to five M and L dwarfs within 10 parsecs of the Sun. *Astron. J.* **128**, 1733 (2004).
91. Burgasser, A. J., Kirkpatrick, J. D. & Lowrance, P. J. Multiplicity among widely separated brown dwarf companions to nearby stars: Gliese 337CD. *Astrophys. J.* **129**, 2849 (2005).
92. Dupuy, T. J., Liu, M. C. & Ireland, M. J. New evidence for a substellar luminosity problem: dynamical mass for the brown dwarf binary Gl 417BC. *Astrophys. J.* **790**, 133 (2014).
93. Dupuy, T. J., Liu, M. C. & Ireland, M. J. Dynamical mass of the substellar benchmark binary HD 130948BC. *Astrophys. J.* **692**, 729 (2009).
94. Nielsen, E. L. et al. The Gemini NICI Planet-Finding Campaign: the frequency of giant planets around young B and A stars. *Astrophys. J.* **776**, 4 (2013).
95. Chen, M. et al. Precise dynamical masses of ε Indi Ba and Bb: evidence of slowed cooling at the L/T transition. *Astron. J.* **163**, 288 (2022).
96. Radigan, J. et al. Discovery of a visual T-dwarf triple system and binarity at the L/T transition. *Astrophys. J.* **778**, 36 (2013).

Acknowledgements J.W.X. thanks S. Mukherjee, T. Dupuy, B. Lacy, C. Morley, J. Fortney, Y. Zhou, G. Hallinan and S. Kulkarni for helpful discussions. J.W.X. acknowledges support for this work through the NASA FINESST Fellowship award 80NSSC23K1434. S.L. acknowledges the support of the French Agence Nationale de la Recherche (ANR) under grants ANR-21-CE31-0017 (project ExoVLTI) and ANR-22-EXOR-0005 (PEPR Origins). M.C.L. acknowledges support from the Gordon and Betty Moore Foundation through grant GBMF8550. J.Wa. acknowledges support from NASA grant 80NSSC23K0280. P.K. acknowledges financing from the European Research Council (ERC) under the European Union's Horizon 2020 research and innovation programme (project UniverScale, grant agreement 951549). P.G. acknowledges the financial support provided by FCT/Portugal through grants PTDC/FIS-AST/7002/2020 and UIDB/00099/2020. This paper is based on observations collected at the European Southern Observatory under ESO programmes 0112.C-2369(A), 0112.C-2369(B) and 2112.D-5036(A). This research has made use of the Jean-Marie Mariotti Center Aspro service available at http://www.jmmc.fr/aspro. This work has benefited from the UltracoolSheet at http://bit.ly/UltracoolSheet, maintained by W. Best, T. Dupuy, M. Liu, A. Sanghi, R. Siverd and Z. Zhang and developed from compilations by ref. 68 and refs. 82–88.

Author contributions J.W.X. led the telescope proposals for Gliese 229, performed the CRIRES+ spectral fitting to obtain radial velocities and wrote the manuscript. A.M., W.T. and D.B. led the closure phase modelling and orbital analysis. Y.Z. reduced the raw CRIRES+ data. S.L. reduced the raw GRAVITY data. D.M., R.O., M.C.L. and A.B. provided advice on the writing and figures. J.K. computed the GRAVITY sensitivity limits. K.B. provided guidance on the system dynamics. A.Sa. performed the analysis with empirical relations. H.K. provided advice on the CRIRES+ spectral fits. R.B.-R. and M.Sa. obtained confirmation Keck/NIRC2 images. The remaining authors constitute the GRAVITY team and commented on the manuscript.

Competing interests The authors declare no competing interests.

Additional information

Correspondence and requests for materials should be addressed to Jerry W. Xuan.

Peer review information *Nature* thanks the anonymous reviewers for their contribution to the peer review of this work.

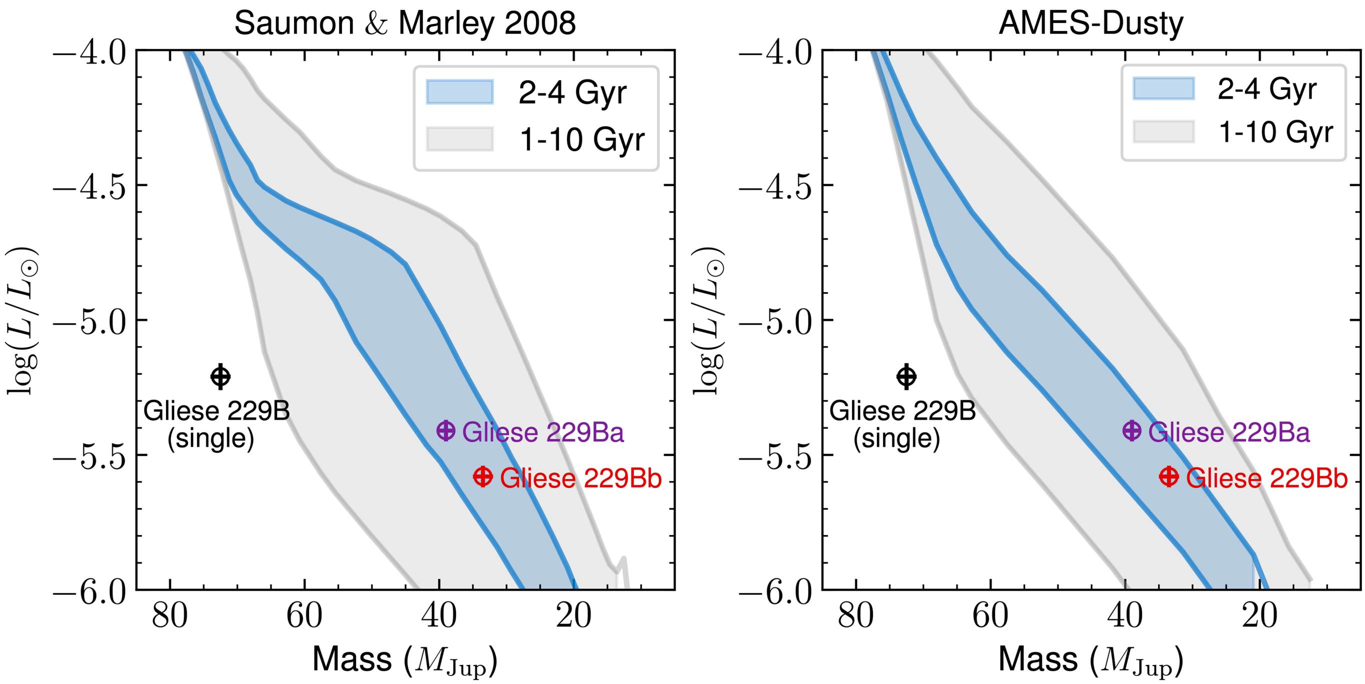

Extended Data Fig. 1 | Dynamical masses and inferred luminosities of Gliese 229 Ba and Bb compared with Saumon and Marley 2008 and AMES-Dusty models. The dynamical masses and estimated luminosities of Gliese 229 Ba (purple) and Bb (red) from the ATMO 2020 evolutionary model fit. As a single brown dwarf, Gliese 229 B is under-luminous compared with model predictions even at 10 Gyr (leftmost grey line). As a binary brown dwarf, the system is consistent with the Saumon and Marley 2008 (ref. 8) and AMES-Dusty[89] models for an age of about 2–4 Gyr.

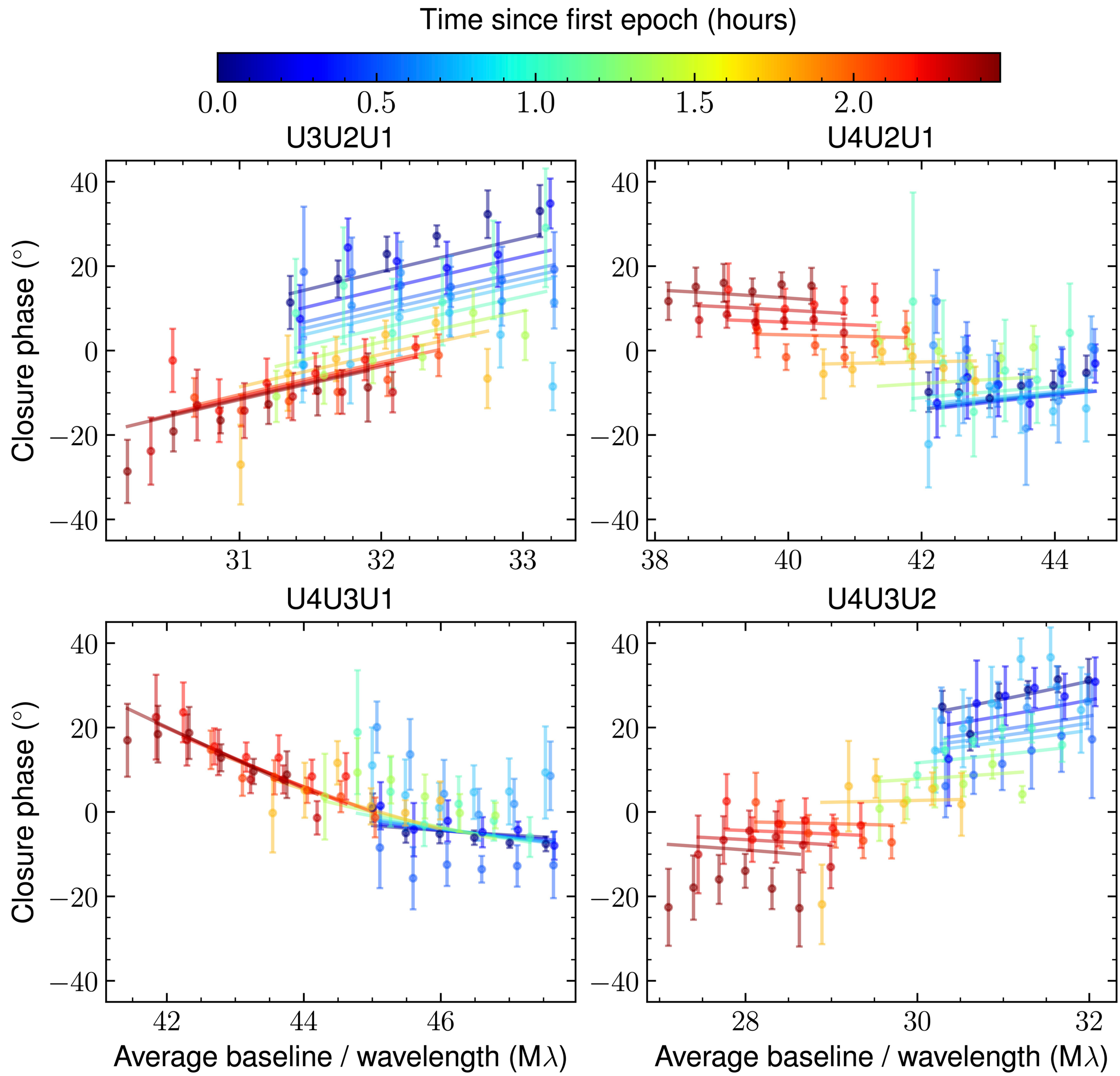

Extended Data Fig. 2 | GRAVITY closure phase measurements of Gliese 229 BaBb on 26 December 2023. The GRAVITY closure phase measurements in the first epoch (26 December 2023). The data are in points and the models are shown as lines. Each panel is for a different baseline triangle between the four Unit Telescopes at the Very Large Telescope (U1, U2, U3, U4). The colour code indicates the time since the first data point (in hours). The data are well described by the model, with most of the residuals at the $<2\sigma$ level. A single source would have zero closure phases throughout.

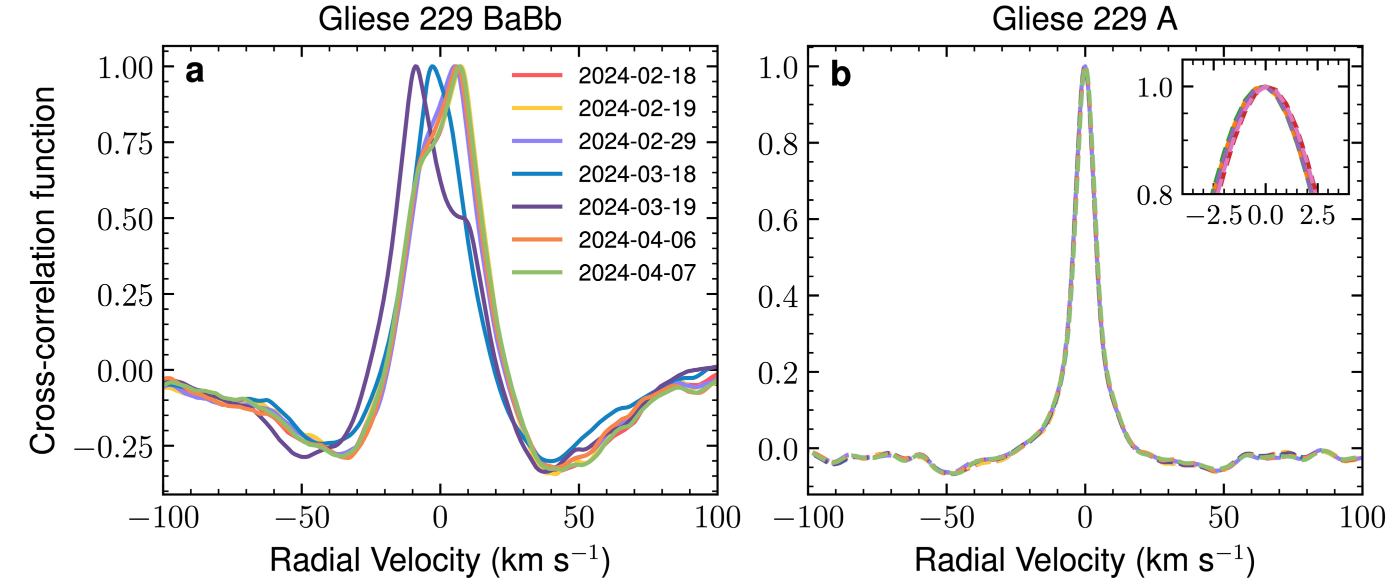

Extended Data Fig. 3 | CCFs of the CRIRES+ spectra of Gliese 229 B and A. **a**, CCFs between the CRIRES+ spectra of Gliese 229 B and an atmospheric model with T_{eff} = 900 K and log(g) = 5.0 computed using Sonora Elf Owl temperature and chemistry profiles. The CCF shapes are distorted and variable over time, characteristic of a double-lined spectroscopic binary. **b**, CCFs between the CRIRES+ spectra of Gliese 229 A and a PHOENIX-ACES model[65] with T_{eff} = 3,800 K and log(g) = 4.5. The inset shows a zoom-in of the CCF peak. The stellar RVs are stable at the 0.1 km s^{-1} level over the observing period, validating the wavelength solution of CRIRES+.

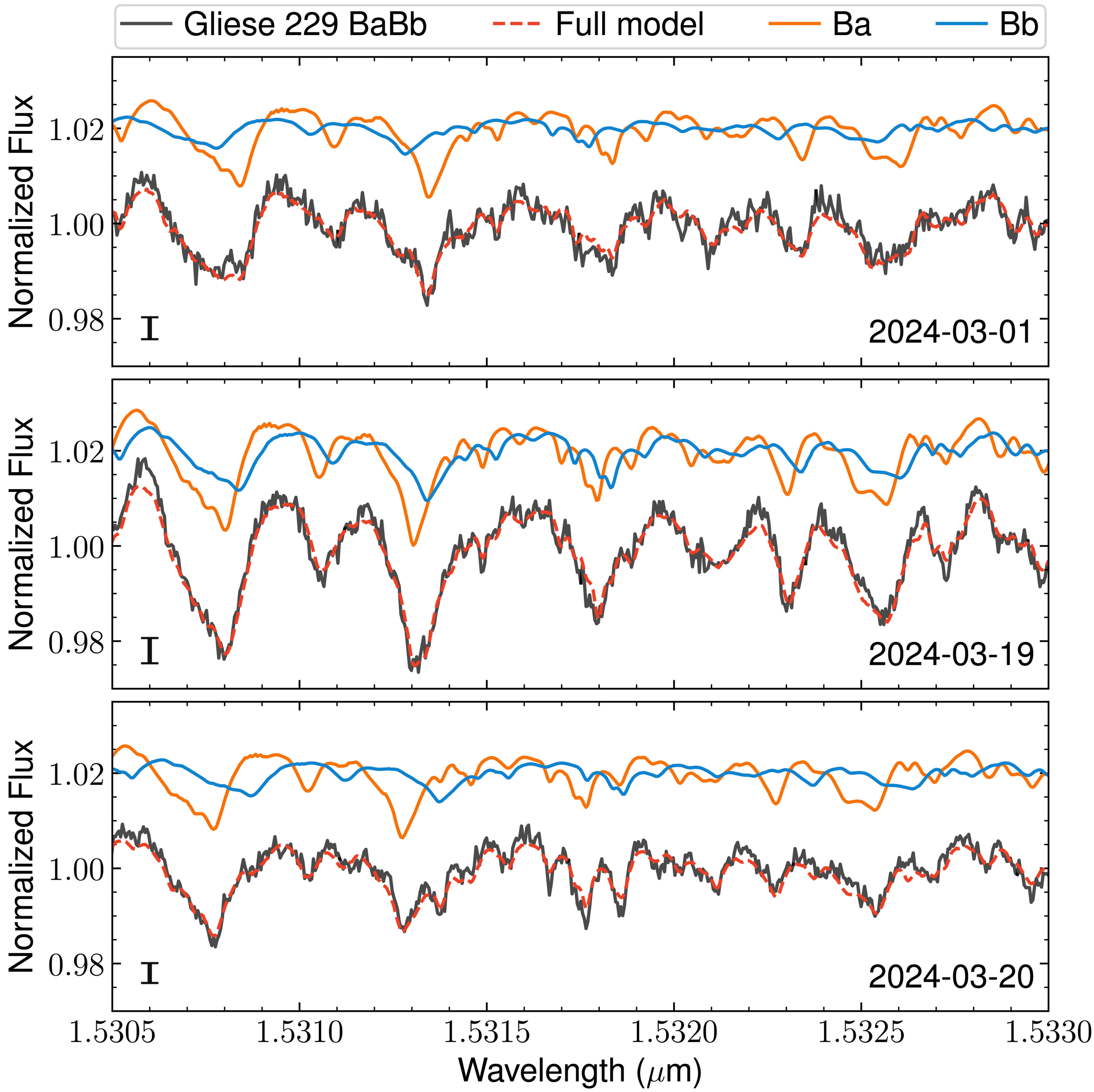

Extended Data Fig. 4 | Zoom-in of the CRIRES+ spectra of Gliese 229 B on three different nights. A small portion of the CRIRES+ spectra on three different nights on which we achieve the highest S/N (black). The Ba and Bb models are shown in orange and blue, respectively, and the full model is in red. The median uncertainties for the spectra are denoted as error bars at the lower left (1σ). Absorption lines from the two brown dwarfs can be seen combining over the observing sequence. The data from 29 March 2024 were taken with the best seeing conditions and consequently contain the highest flux from the brown dwarfs and minimal stellar contamination from Gliese 229 A. Therefore, the lines appear deeper for this epoch.

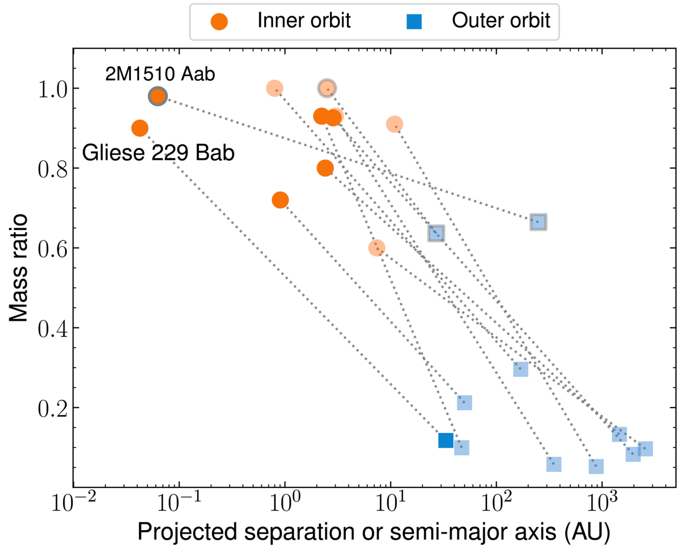

Extended Data Fig. 5 | Gliese 229 A-Bab and other binary brown dwarfs in triple systems. For each system, we show the orbital separation and mass ratio of the binary brown dwarf in orange. The separation of the outer orbit (that is, between the brown dwarfs and the third component) and mass ratio of the binary brown dwarf relative to the total system mass is in blue. Many systems have prohibitively long orbital periods or lack published orbit solutions; we use transparent points to denote projected separations and opaque points for measured semimajor axes. Each system is connected with a grey dotted line. We label the similarly tight binary 2M1510 Aab from ref. 30. The circles with grey outlines are triple brown dwarf systems, in which all components are substellar. Among binary brown dwarfs orbiting stars, Gliese 229 Bab has an inner orbit more than an order of magnitude smaller than other systems. The parameters for other systems are taken from refs. 24,84,90–96.

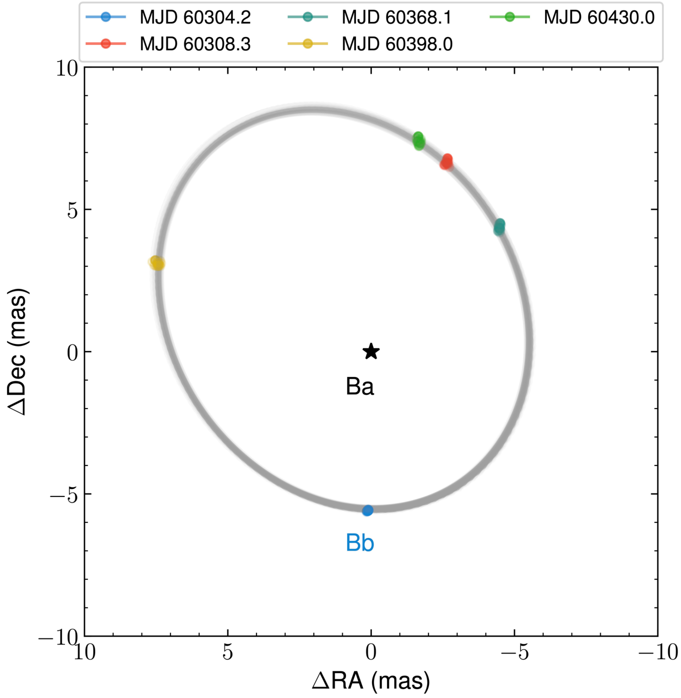

Extended Data Fig. 6 | Relative orbit of Gliese 229 Bb with respect to Gliese 229 Ba from GRAVITY and CRIRES+. Random draws of the relative astrometric orbit of Gliese 229 Ba-Bb from the PMOIRED fit are shown as grey curves. The position of the primary brown dwarf Gliese 229 Ba is marked with a star at the origin. The coloured points show random draws of the predicted astrometric positions of Bb with respect to Ba from the joint GRAVITY and CRIRES+ orbit fit over the five observing epochs.

Extended Data Table 1 | GRAVITY Wide and CRIRES+ observation log for Gliese 229 BaBb

Instrument	DATE START (UT)	DATE END	NEXP/NDIT/DIT(seconds)	AIRMASS	TAU0 (milli-second)	SEEING (arcsec)
GRAVITY Wide	2023-12-26T04:14:07	2023-12-26T06:48:36	13/4/100	1-1.16	5-20	0.5-1.1
GRAVITY Wide	2023-12-30T05:47:25	2023-12-30T06:32:50	4/4/100	1.1-1.2	5-10	0.4-0.8
GRAVITY Wide	2024-02-28T02:57:39	2024-02-28T03:36:49	3/4/100	1.2-1.4	5-6	0.7-0.9
GRAVITY Wide	2024-03-29T00:31:24	2024-03-29T01:17:35	4/4/100	1.1-1.3	8-12	0.4-0.6
GRAVITY Wide	2024-04-29T23:15:22	2024-04-29T23:29:21	2/4/100	1.3-1.4	4-10	0.7-0.8
CRIRES+	2024-02-19 T02:27:37	2024-02-19 T04:10:34	6/1/900	1.1-1.4	7-18	0.6-1.15
CRIRES+	2024-02-20T02:22:28	2024-02-20T03:00:26	2/1/900	1.1	5-7	0.8-1.5
CRIRES+	2024-03-01T01:45:04	2024-03-01T03:28:13	6/1/900	1.1-1.4	7-9	0.5-0.8
CRIRES+	2024-03-19T00:54:23	2024-03-19T02:37:11	6/1/900	1.1-1.5	6-8	0.4-0.7
CRIRES+	2024-03-20T00:36:04	2024-03-20T02:18:21	6/1/900	1.1-1.4	2-6	0.6-0.7
CRIRES+	2024-04-07T00:12:23	2024-04-07T01:12:00	4/1/600	1.2-1.4	4-6	0.6-0.9
CRIRES+	2024-04-08T23:31:31	2024-04-08T00:24:28	4/1/600	1.1-1.2	7-8	0.7-1.0

We provide the observation times, exposure settings, and observing conditions for each epoch of observation.

Extended Data Table 2 | Bulk properties of Gliese 229 BaBb inferred from the ATMO 2020 evolutionary model

Parameter	ATMO 2020
Mass ratio	0.87±0.03
Age (Gyr)	2.45±0.20
$T_{eff,Ba}$ (K)	860±20
$T_{eff,Ba}$ (K)	770±20
$\log(g)_{Ba}$ (dex)	5.11±0.01
$\log(g)_{Bb}$ (dex)	5.03±0.01
$\log(L/L_{\odot})_{Ba}$	-5.41±0.04
$\log(L/L_{\odot})_{Bb}$	-5.58±0.04

Extended Data Table 3 | RVs of Gliese 229 Ba and Bb from VLT/CRIRES+

Time (MJD)	RV_{Ba} (km/s)	RV_{Bb} (km/s)
60359.14	8.07±0.12	-7.51±0.19
60360.11	8.13±0.14	-7.22±0.19
60370.11	6.07±0.17	-6.31±0.25
60388.07	-3.21±0.54	4.09±0.75
60389.058	-8.97±0.23	10.60±0.46
60407.03	6.85±0.16	-7.55±0.24
60408.00	7.49±0.27	-8.10±0.32

Extended Data Table 4 | Derived relative astrometry of Gliese 229 Ba-Bb from the Octofitter fit

Date [UTC]	Projected separation [mas]	Position Angle [deg]	Separation [AU]
2023-12-26 05:15:42	5.58± 0.01	178.4 ± 0.9	0.0338 ± 0.0001
2023-12-30 06:11:23	7.10±0.05	-22.0± 0.1	0.0453±0.0002
2024-02-28 03:13:29	6.19±0.04	-46.5± 0.3	0.0413±0.0001
2024-03-29 00:31:14	7.95± 0.03	67.6 ±0.5	0.0488±0.0001
2024-04-29 23:15:12	7.49± 0.04	-13.5± 0.2	0.0468±0.0002

As noted in Methods, these values should not be used directly in orbit fits.